PAPER

A rhodamine-based chemosensor with diphenylselenium for highly selective fluorescence turn-on detection of Hg^{2+} *in vitro* and *in vivo*†

Parthiban Venkatesan, Natesan Thirumalivasan and Shu-Pao Wu [ID] *

A rhodamine-B based chemosensor with diphenylselenium, **RhoSe**, has been synthesized, and its detection behavior towards various metal ions is studied *via* UV/Vis and fluorescence spectroscopy. **RhoSe** shows a selective response to Hg^{2+} in CH$_3$OH/H$_2$O (v/v = 9 : 1) solutions over other metal ions. After addition of Hg^{2+}, the solution of **RhoSe** displays an obvious color change from colorless to pink and a significant, 48-fold fluorescence enhancement. The color change and fluorescence enhancement are attributed to the ring-opening of the spirolactam in the rhodamine fluorophore, which is induced by Hg^{2+} binding. The binding ratio of **RhoSe**–Hg^{2+} was determined by a Job plot as a 1 : 1 ratio, and the effective pH range for Hg^{2+} detection was 4.0–10. Importantly, the reversibility of the **RhoSe**–Hg^{2+} complex was observed through the addition of Na$_2$S. For practical applications, the strip method was utilized to detect Hg^{2+} in water/methanol solution. In addition, confocal fluorescence microscopy experiments demonstrated that **RhoSe** is an effective fluorescent probe for Hg^{2+} detection *in vitro* and *in vivo*.
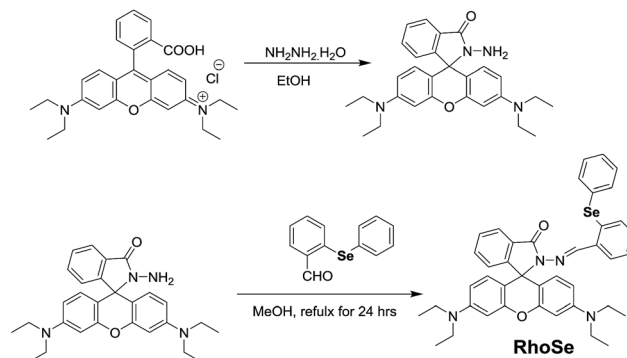
Introduction

There is a growing demand to develop selective and sensitive chemosensors for toxic metal ions in environmental and biological studies.[1–4] Mercury is known as a highly toxic heavy metal even at very low concentrations. Mercury can be found in various products, such as batteries, light bulbs, and thermometers. Three forms of mercury exist: metallic mercury, ionic mercury, and organic mercury. Metallic mercury can be converted into methylated forms, mainly methylmercury and dimethylmercury, by bacteria.[5,6] Mercury ions show high affinities with the thiol groups in proteins, and their accumulation in the body has harmful effects on the brain, central nervous system, and kidneys. Minamata disease, discovered in Minamata city, Japan, is a typical disease caused by severe mercury poisoning.[7] Due to the high toxicity of mercury, the highest permitted concentration of mercury in environmental and dietary samples has been established by the EPA in the USA as 2 ppb.[8]

Many analytical methods for mercury determination in environmental and clinical samples have been developed, such as inductively coupled plasma atomic emission spectrometry (ICP-AES),[9] atomic absorption spectroscopy (AA),[10] electrochemical method[11] and inductively coupled plasma mass

spectrometry (ICP-MS).[12] Fluorescence chemosensors provide a direct way for mercury detection due to their high sensitivity, selectivity, and their applications in environmental and biological analysis.[13–25] Among various available fluorophores, rhodamine is remarkable due to its exceptional optical properties, such as a long absorption and emission wavelength, high extinction coefficient and quantum yield, and low detection limit.[4,26] Furthermore, rhodamine exists in two forms, a spirolactam (non-fluorescent) form and a ring-opened amide (fluorescent) form, providing an ideal model for the design of metal ion sensing with light "off–on" switching. Binding metal ions to rhodamine derivative induces ring-opening of rhodamine. This resulted in a red emission and a color change from colorless to pink because of a shift in the equilibrium state from a spirolactam to a ring-open amide.[27–35]

Department of Applied Chemistry, National Chiao Tung University, Hsinchu 300, Taiwan. E-mail: spwu@mail.nctu.edu.tw; Fax: +886-3-5723764; Tel: +886-3-5712121 ext 56506

Scheme 1 Synthesis route of **RhoSe**.

In this work, a chemosensor **RhoSe** containing a rhodamine B hydrazide linked with diphenyl selenium was synthesized for Hg^{2+} detection (Scheme 1). Due to its spirolactam form, **RhoSe** has no visible absorption and is colorless. The binding of Hg^{2+} to the chemosensor **RhoSe** induced a switch from the spirolactam form to the ring-opened amide form, which was observed as a pink color. More importantly, **RhoSe** could potentially be applied to test strips, living cell imaging, and zebrafish studies.

Results and discussion

Synthesis of RhoSe

The chemosensor **RhoSe** was synthesized by the reaction of rhodamine B hydrazide and 2-(phenylselanyl) benzaldehyde to form a Schiff base (Scheme 1). **RhoSe** was characterized by ^{1}H NMR, ^{13}C NMR, and HRMS (ESI) (see the ESI†).

The selectivity towards metal ions measured by UV-visible and fluorescence spectra

The metal ion detection ability of chemosensor **RhoSe** was further evaluated. Fig. 1 shows the metal ion selectivity of **RhoSe**; only Hg^{2+} causes a color change and produces a yellow fluorescence. Other metal ions cause no change in the fluorescence and color. Fig. 2 shows the UV/Vis and fluorescence spectra of chemosensor **RhoSe** in the presence of several metal ions. Only Hg^{2+} caused significant absorption and emission peaks at 561 and 584 nm, respectively. Hg^{2+} titration of chemosensor **RhoSe** was monitored by UV/Vis spectra (Fig. 3a). During the sequential addition of Hg^{2+} ions, a new absorption band at 561 nm was observed with an intense pink color. Free **RhoSe** does not exhibit any absorption peak in the visible region due to its spirocyclic form. When **RhoSe** binds with Hg^{2+}, the binding induces the ring-opening of rhodamine, resulting in the pink color. During Hg^{2+} titration, an emission peak at 584 nm was produced (Fig. 3b). Based on the fluorescence titration profile, the detection limit of **RhoSe** for the Hg^{2+} ion was calculated to be 12 nM (see Fig. S5 in the ESI†).

In order to quantify the effective fluorogenic change, a quantum yield calculation was carried out. The quantum yield of **RhoSe** was found to be as low as $\Phi = 0.006$. Upon coordination with Hg^{2+}, the quantum yield of **RhoSe**–Hg^{2+} was $\Phi = 0.29$, which is a 48-fold enhancement. Next, the binding ratio of
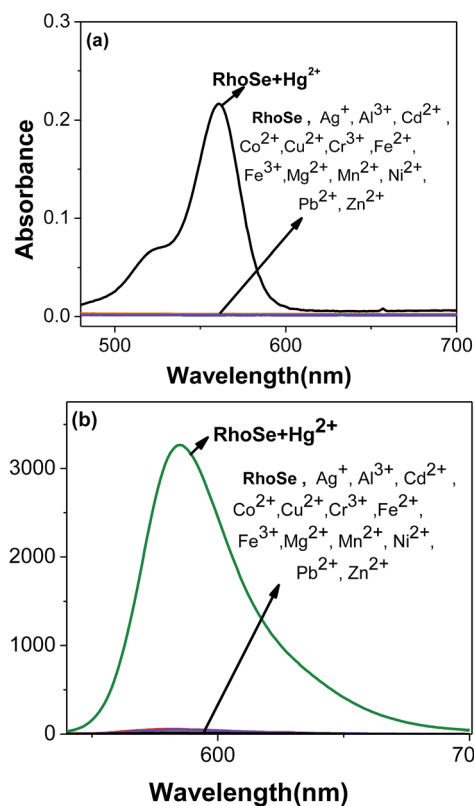

Fig. 2 Absorption and fluorescence spectra of **RhoSe** (10.0 μM) in the presence of different metal ions in CH_3OH/H_2O (v/v = 9 : 1) solution.
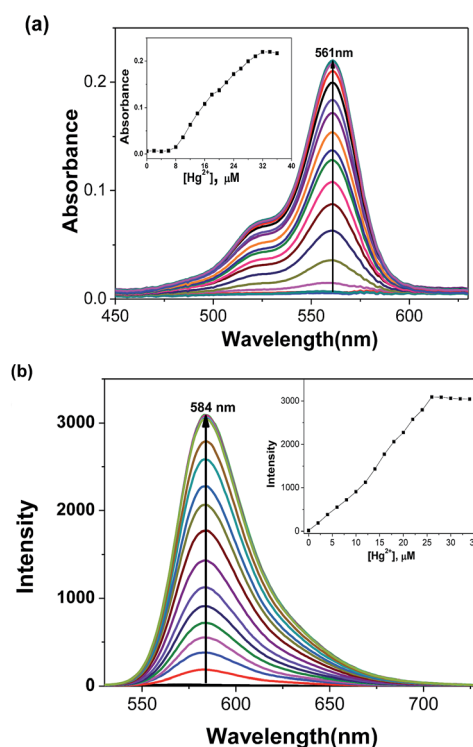

Fig. 3 Absorption and fluorescence titration spectra of **RhoSe** (10 μM) with gradual addition of Hg^{2+} in CH_3OH/H_2O (v/v = 9 : 1) solution.
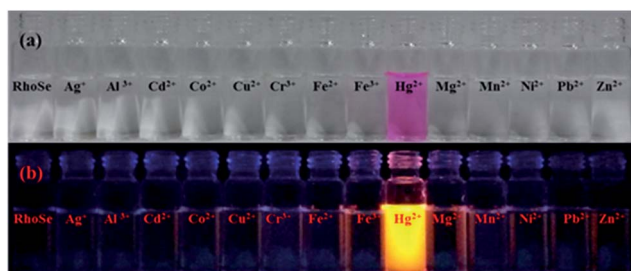
Fig. 1 (a) Color and (b) fluorescence changes of **RhoSe** (100 μM) with metal ions (100 μM) in CH_3OH/H_2O (v/v = 9 : 1) solution.

RhoSe–Hg^{2+} was evaluated by Job plot experiments. The fluorescence intensity at 584 nm was plotted against the molar fraction of **RhoSe**. The highest fluorescence intensity was reached at a molar fraction of 0.5, indicating that **RhoSe** binds to Hg^{2+} with a 1 : 1 ratio (see Fig. S6 in the ESI†). ESI mass spectra also provided further support for a 1 : 1 metal complex, with $m/z = 1002.13$ (see Fig. S7 in the ESI†). Furthermore, the binding constant was obtained as 7.44×10^4 M^{-1}, which indicates the strong binding affinity of **RhoSe** for the Hg^{2+} ion (see Fig. S8 in the ESI†).

To further evaluate the influence of other metal ions, experiments with coexisting ions were carried out. **RhoSe** (10 μM) was examined with various metal ions in the presence of Hg^{2+}. As shown in Fig. 4a, the fluorescence intensity with coexisting ions is similar to that from Hg^{2+} alone. This observation indicates that there was no interference from the other metal ions. Owing to the importance of pH, we also studied the emission behavior of **RhoSe** towards the Hg^{2+} ion with respect to different pH environments. As shown in Fig. 4b, only a low emission intensity was observed for **RhoSe** at pH 4.0–10.0. When the pH is lower than 4, the emission intensity increases remarkably; this is due to the protonation-induced ring opening in **RhoSe**. With Hg^{2+}, a high emission intensity at 584 nm was

observed at pH 4.0–10. Furthermore, the emission intensity of **RhoSe** decreased slightly when the pH was higher than 10.0. This is due to the reduced stability of **RhoSe**–Hg^{2+} at high pH values. These observations confirm that **RhoSe** can be used to detect Hg^{2+} over a wide pH range. In order to examine the reversibility of **RhoSe**–Hg^{2+}, Na$_2$S was added to remove the Hg^{2+}. In Fig. 5, the emission peak at 584 nm decreased after the addition of Na$_2$S. With further addition of Hg^{2+}, the fluorescence of **RhoSe**–Hg^{2+} was regained. The collective data clearly indicates the reversible binding character of the chemosensor **RhoSe** to Hg^{2+}.

We further performed Hg^{2+} titrations monitored by ^{1}H NMR to determine the binding interaction between **RhoSe** and Hg^{2+}. As a heavy metal ion, Hg^{2+} affects the proton signals near the Hg^{2+} binding site.[36] The ^{1}H NMR signal of the imine nitrogen proton (–CH=N) was shifted upfield upon the addition of Hg^{2+} (Fig. 6). Two protons signals, H^b and H^f, which are located adjacent to the selenium atom on the diphenyl-selenium moiety, were also shifted upfield and became much broader after the sequential addition of Hg^{2+} ions. Furthermore, the IR spectra of **RhoSe** and **RhoSe**–Hg^{2+} were recorded (Fig. 7). Without Hg^{2+}, two peaks at 1715 cm^{-1} and 1684 cm^{-1} are the strength mode of the carbonyl oxygen (C=O). After addition of
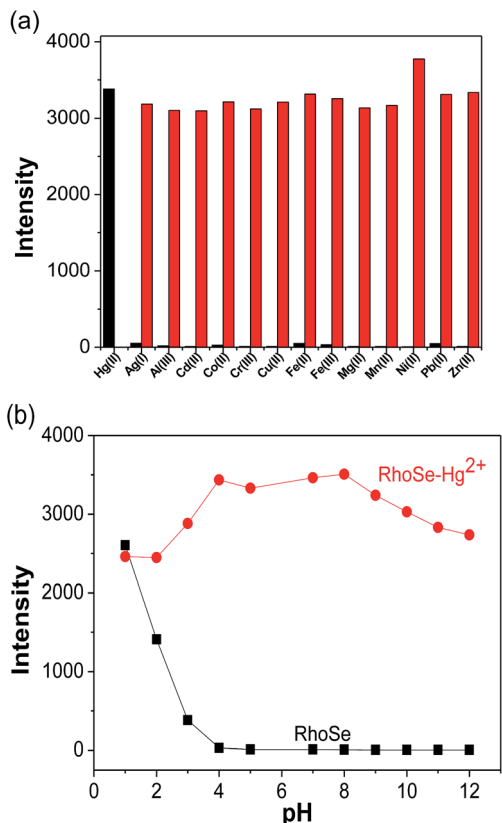

Fig. 4 (a) Fluorescence intensity at 584 nm of **RhoSe** (10 μM) with various metal ions in CH$_3$OH/H$_2$O (v/v = 9 : 1) solution. The black bars represent single metal ion (30 μM); the red bars represent coexisting metal ion:Hg^{2+} (30 μM) + other metals (60 μM). (b) Fluorescence intensity at 584 nm of **RhoSe** (10 μM) with Hg^{2+} (30 μM) at different pH in CH$_3$OH/H$_2$O (v/v = 9 : 1) solutions. The excitation wavelength was 510 nm.
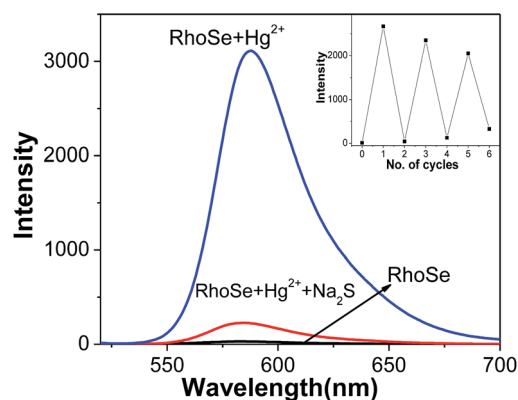
Fig. 5 Reversible binding of **RhoSe** with Hg^{2+}. **RhoSe** was added with Hg^{2+} (30 μM) and Na$_2$S (30 μM).
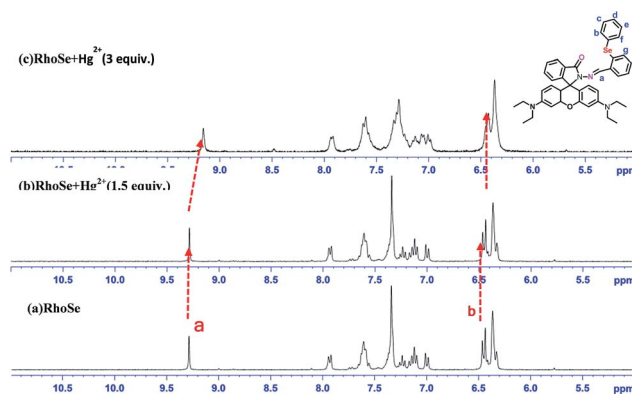

Fig. 6 ^{1}H NMR (300 MHz) spectra of **RhoSe** in the presence of Hg^{2+} in DMSO-d$_6$.
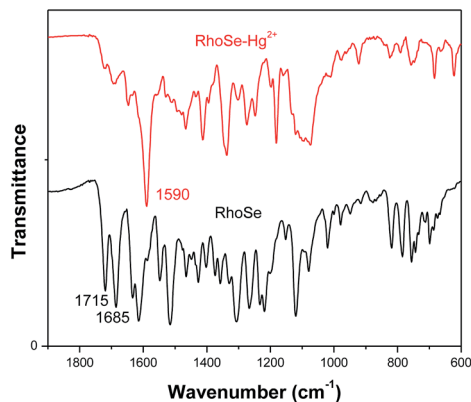
Fig. 7 FT IR spectra of **RhoSe** and **RhoSe** + Hg^{2+}.

Scheme 2 Proposed Hg^{2+} binding mechanism of **RhoSe**.

Fig. 8 DFT-optimized structures of (a) **RhoSe** and (b) **RhoSe**−Hg^{2+} complex using the B3LYP/LanL2DZ method. Black atom, C; blue atom, N; red atom, O; yellow atom, Se; gray atom, Hg.
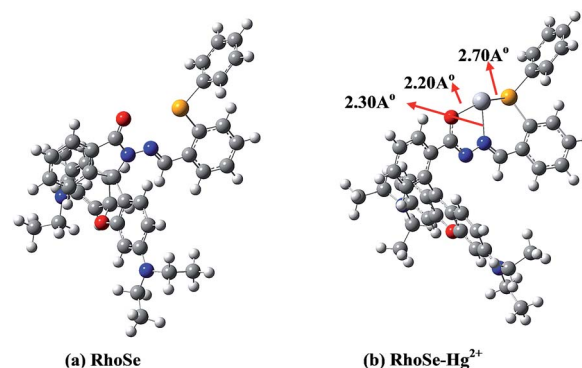
Hg^{2+} ions, the peak corresponding to the carbonyl oxygen (C= O) in rhodamine disappeared. In addition, a new stretching frequency at 1618 cm^{-1} (C=N) is corresponding to its ring opened amide conformation. The collective data indicates that Hg^{2+} binds to **RhoSe** through the selenium atom at a diphenyl-selenium moiety, one nitrogen atom, and one oxygen atom. Some recently reported fluorescence Hg^{2+}-sensors based on rhodamine derivatives are shown in Table 1. Some rhodamine based Hg^{2+} sensors show response to Hg^{2+} and the other metal ions, such as Cu^{2+} and Zn^{2+}. The probe **RhoSe** only responses to Hg^{2+} with a low detection limit 12 nM. Also, the probe **RhoSe** can be applied in test strip detection and bioimaging in cells and zebrafish.

According to the collective results, the binding mechanism is shown in Scheme 2. When the probe **RhoSe** is in the spirolactam form, it has no visible absorption and is colorless. Upon the complexation of **RhoSe** with Hg^{2+}, Hg^{2+} binding induced a switch from the spirolactam form to the ring-opened amide form, which was observed as a pink color.

In order to elucidate the structures of **RhoSe** and **RhoSe**– Hg^{2+}, density functional theory (DFT) calculations using the Gaussian 09 software package were carried out. We applied the B3LYP/LANL2DZ energy optimization to determine the optimal structures of **RhoSe** and **RhoSe**–Hg^{2+} (Fig. 8). The structure of

RhoSe–Hg^{2+} shows that Hg^{2+} binds to the chemosensor **RhoSe** by one nitrogen atom, one oxygen atom, and one selenium atom at distances of 2.30, 2.20, and 2.70 Å, respectively. The energy gaps between the HOMO and LUMO levels of **RhoSe** and **RhoSe**– Hg^{2+} are ΔE = 3.81 eV and 1.08 eV, respectively (see Fig. S9 in the ESI†). **RhoSe**–Hg^{2+} has a smaller energy gap compared with that of **RhoSe**.

Application of RhoSe in test strips

To apply the chemosensor **RhoSe** to a practical use, test strips were prepared by immersing filter paper in **RhoSe** solution,

Table 1 Comparison of analytical methods for determination of Hg^{2+} by rhodamine derivatives

| Materials	Methods/analyte (LOD)	Solvent	Comments	Ref.
Rhodamine derivative	Fluorescence on Cu^{2+} (1.63 μM) Hg^{2+} (2.36 μM)	EtOH/H$_2$O (10 mM HEPES, pH 7.4) 4 : 1	Response to Cu^{2+} and Hg^{2+}, cell imaging	27
Rhodamine derivative	Fluorescence on Hg^{2+} (0.067 μM)	EtOH/H$_2$O (1/1, v/v)	High selectivity	28
Rhodamine derivative	Fluorescence on Hg^{2+} (3.2 nM)	EtOH/H$_2$O (1/1, v/v)	High selectivity, cell imaging	29
Rhodamine derivative	Fluorescence on Hg^{2+}	EtOH–H$_2$O (8 : 2 v/v, PBS, pH 7.1)	High selectivity	30
Rhodamine derivative	Fluorescence on Zn^{2+} (2.21 μM) Hg^{2+} (2.16 μM)	CH$_3$CN/H$_2$O (HEPES, 2.5 mM, pH 7) 8 : 2	Response to Zn^{2+} and Hg^{2+}, cell imaging	31
Rhodamine derivative	Fluorescence on Hg^{2+} (32 nM)	CH$_3$CN/H$_2$O 1 : 1	Response to Cu^{2+} and Hg^{2+}	32
Rhodamine derivative	Fluorescence on Hg^{2+} (9.32 nM) Uric acid (15.4 nM)	CH$_3$OH/H$_2$O (phosphate, pH 7.0) 1 : 2	Response to Hg^{2+} and uric acid, cell imaging	33
Rhodamine derivative	Fluorescence on Hg^{2+} (12 nM)	CH$_3$CN/H$_2$O 9 : 1	Highly selective and sensitive, good reversibility, strip method and used *in vitro* and *in vivo*	This work
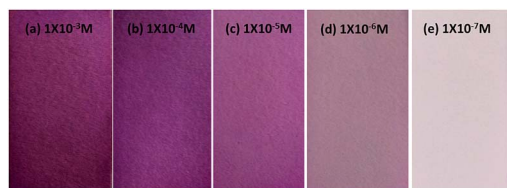
Fig. 9 Colorimetric test strips of **RhoSe** (1 mM) with Hg^{2+}. (a) 1×10^{-3} M, (b) 1×10^{-4} M, (c) 1×10^{-5} M, (d) 1×10^{-6} M, (e) 1×10^{-7} M.

followed by drying in air. The selectivity of the test strips for various metal ions was first evaluated (see Fig. S10 in the ESI†). Only in the presence of Hg^{2+} were a pink color and yellow emission observed; other metal ions did not cause any color or fluorescence changes in the test strips. In addition, the test strips were immersed in different concentrations of Hg^{2+}, and exhibited a clear color change from colorless to pink with increasing Hg^{2+} concentration (Fig. 9). The detection limit of the test strips was found to be 1×10^{-6} M, allowing for sensitive detection of Hg^{2+} ions.

Bioimaging of RhoSe

The bioimaging potential of **RhoSe** for Hg^{2+} was further explored. Firstly, the cytotoxicity of **RhoSe** was evaluated by an MTT assay using HeLa cells. The cellular viability of HeLa cells treated with **RhoSe** was greater than 80%, which indicates a low cytotoxicity of **RhoSe** (<20 μM) (see Fig. S11 in the ESI†). Thereafter, **RhoSe** was applied to image Hg^{2+} using confocal fluorescence microscopy. Fig. 10a shows that no fluorescence was observed from HeLa cells treated with **RhoSe**. With Hg^{2+}, a bright red fluorescence emission in the HeLa cells can be clearly observed (Fig. 10b). The overlay image revealed that the red fluorescence was distributed throughout the intracellular area. This observation shows the good cell-membrane permeability of **RhoSe**.

Fluorescence imaging experiments of RhoSe in zebrafish

Furthermore, **RhoSe** was used for Hg^{2+} imaging in zebrafish. First, 3 day-old fish were treated with the chemosensor **RhoSe** (20 μM) for 30 min at 28 °C. No red fluorescence was found (Fig. 11a). With Hg^{2+}, a strong red fluorescence in the 3 day-old
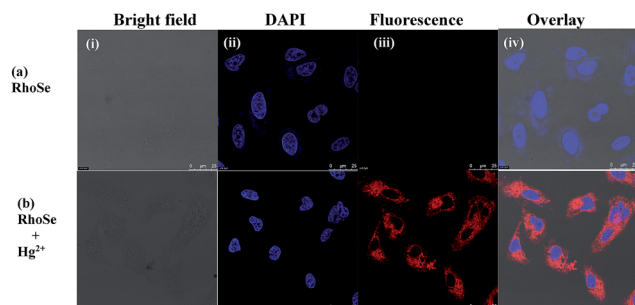

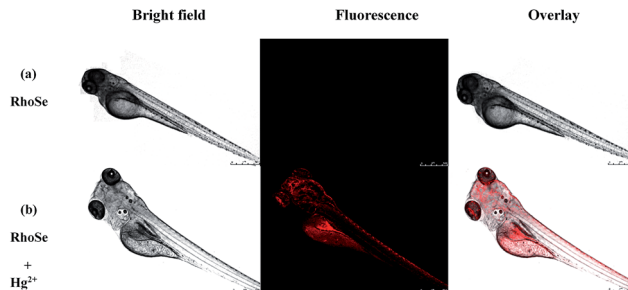**Fig. 10** Confocal microscopy images of **RhoSe** treated with Hg^{2+} ions in HeLa cells.

Fig. 11 Confocal microscopy images of 3 day-old zebrafish. (a) The zebrafish incubated with **RhoSe** (20 μM) for 30 min. (b) Subsequent treatment with Hg^{2+} (60 μM) for 30 min.
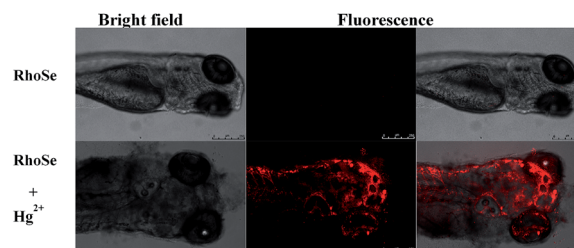

Fig. 12 Hg^{2+} accumulation and distribution in 3 day-old zebrafish brain.

zebrafish was observed (Fig. 11b). Remarkably, the organs in the zebrafish, such as the heart, liver, and brain, were clearly seen.[37,38] In addition, a lower fluorescence intensity was observed in the brain (Fig. 12). This indicates a relatively lower level of mercury in the brain. The zebrafish fluorescent images demonstrate that the chemosensor **RhoSe** can be used to study the accumulation of mercury species *in vivo*.

Experimental

Instruments

Hitachi F-7000 fluorescence spectrophotometer was used for fluorescence spectra measurements. ^1H and ^{13}C NMR spectra were obtained with a 300 MHz Bruker spectrometer. UV/Vis spectra were recorded on an Agilent 8453 UV/Vis spectrometer. Fluorescence microscope images were obtained from a Leica TCS SP5 X AOBS Confocal Fluorescence Microscope.

Synthesis of RhoSe

Rhodamine B hydrazide[39] (500 mg, 1.0 mmol) and 2-(phenylselanyl) benzaldehyde[40] (314 mg, 1.1 mmol) were added to methanol (20 mL). The reaction mixture was refluxed for 24 h. The subsequent precipitate was filtrated and column chromatography (DCM: hexane = 1 : 1) was used to purify the compound. Yield: 698 mg (89%). Melting point: 178–180 °C. ^1H NMR (300 MHz, DMSO-d_6): δ 9.28 (s, 1H), 7.93 (d, 1H, $J = 7.2$ Hz), 7.60 (t, 3H, $J = 6.3$ Hz), 7.33 (s, 4H), 7.23 (t, 3H, $J = 7.5$Hz), 7.16–7.09 (m, 2H), 7.0 (d, 1H, $J = 7.8$Hz), 6.51–6.28 (m, 7H), 3.25 (q, 8H, $J = 6.6$ Hz), 1.01 (t, 12H, $J = 6.6$ Hz); ^{13}C NMR (75 MHz, DMSO-d_6): 164.2, 153.1, 152.0, 149.0, 148.8, 135.2, 134.5, 134.4, 134.1, 131.9, 130.7, 130.5, 130.0, 129.2, 129.0, 128.7, 128.3,

126.8, 124.3, 123.4, 108.5, 105.5, 97.9, 66.0, 44.1, 12.7. MS (ESI): $m/z = 701.2$ ([M + H]$^+$); HRMS (ESI): calcd for $C_{41}H_{41}N_4O_2Se$ ([M + H]$^+$) 701.2354; found 701.2390.

Binding stoichiometry and the association constant (K_a) of RhoSe with Hg^{2+}

Job plot was used to decide the binding ratio of the complex **RhoSe**–Hg^{2+}. The molar fraction of **RhoSe** was plotted against the fluorescence intensity at 584 nm. The total concentration of **RhoSe** and Hg^{2+} was 50 μM. The binding stoichiometry of the complex **RhoSe**–Hg^{2+} was determined from the molar ratio with maximum fluorescence intensity. The association constant (K_a) of the complex **RhoSe**–Hg^{2+} was obtained by using the Benesi–Hilderbrand equation.[41]

$$1/\Delta F = 1/\Delta F_{sat} + 1/(\Delta F_{sat} K_a [Hg^{2+}]) \qquad (1)$$

where ΔF is the intensity difference at 584 nm and ΔF_{sat} is the maximum intensity difference at 584 nm. The plot ($1/\Delta F$ *vs.* $1/[Hg^{2+}]$) was fitted by using eqn (1) and the association constant K_a was obtained from the intercept and slope of the line.

Cytotoxicity assay

The cytotoxicity of **RhoSe** was determined by the methyl thiazolyl tetrazolium (MTT) assay. HeLa cells were grown in Dulbecco's modied Eagle's medium (DMEM) with 10% fetal bovine serum (FBS) at 37 °C, 5% CO$_2$. Then HeLa cells were grown into a 96-well cell-culture plate. The cells were added with several concentrations (5, 10, 15, 20, 25 μM) of **RhoSe** and then incubated at 37 °C, 5% CO$_2$ for 24 h. Subsequently, each well was added with MTT (10 μL, 5 mg mL^{-1}) and then incubated at 37 °C, 5% CO$_2$ for 4 h. Yellow precipitates (formazan) formed in plates then were collected and dissolved in DMSO (200 μL) and Sorenson's glycine buffer (25 μL, 0.1 M glycine and 0.1 M NaCl). The absorbance at 570 nm of each well was recorded by Multiskan GO microplate reader. Cell viability was calculated by the following equation:

Cell viability (%) = (average absorbance of treatment group)/ (average absorbance of control group).

Fluorescence imaging of RhoSe

HeLa cells were treated with Hg(ClO$_4$)$_2$ (30 μM, dissolved in PBS) and incubated for 30 min at 37 °C. Excess metal ions were washed away by PBS (3 × 2 mL). The cells were added with culture media (2 mL) and then incubated with **RhoSe** (10 μM, dissolved in DMSO). After 30 min incubation at 37 °C, the culture media was removed and cells were washed with PBS (3 × 2 mL). Cell imaging was obtained by a Leica TCS SP5 X AOBS Confocal Fluorescence Microscope (Germany) with the excited wavelength, 510 nm and the collected emission at 580–590 nm.

Hg^{2+} imaging in zebrafish

Animals were maintained in accordance with the guidelines of the National Institute of Health, Taiwan, and approved by the Institutional Animal Care and Use Committee (IACUC) of National Chiao Tung University. Zebrafish was kept at best breeding conditions at 28 °C. For mating, male and female zebrafish were put in the same tank at 28 °C in a 12 h light/12 h dark cycle. The spawning of eggs was triggered by light stimulation in the morning. Most eggs were fertilized immediately. The zebrafish was growed in 5 mL of embryo medium supplemented with 1-phenyl-2-thiourea (PTU) in 6-well plates for 24 h at 28 °C. Furthermore, 3 day-old zebrafish embryos were anaesthetized with 50 mg L^{-1} tricaine and incubated with mercury(II) perchlorate hydrate (60 μM) in E3 media for 30 min at 28 °C. PBS buffer was used to remove the remaining mercury ions. The zebrafish was further incubated with **RhoSe** (20 μM) for 30 min at 28 °C. After washing with PBS to remove the remaining probe, the image of zebrafish was observed by a Leica TCS SP5 X AOBS Confocal Fluorescence Microscope.

Computational methods

Quantum chemical calculations based on density functional theory (DFT) were carried out using a Gaussian 09 program. The optimal structures of **RhoSe** and **RhoSe**–Hg^{2+} were obtained using the density functional theory (DFT) method with the hybrid-generalized gradient approximation (HGGA) functional B3LYP. For **RhoSe**–Hg^{2+}, the LANL2DZ basis set was used for Hg^{2+}, whereas the 6-31G basis set was used for **RhoSe**.

Conclusions

In conclusion, a rhodamine-based probe **RhoSe** with diphenylselenium has been designed for selective and sensitive Hg^{2+} detection. **RhoSe** showed a rapid response to Hg^{2+} alone among other metal ions, with colorimetric and fluorescent turn-on responses. **RhoSe** can be used for Hg^{2+} detection over a pH range of 4.0–10.0. In addition, the stoichiometry of the **RhoSe**–Hg^{2+} complex was calculated as a 1 : 1 binding ratio using a Job plot, and was further confirmed by ESI-MS. **RhoSe** shows high sensitivity towards Hg^{2+} with a detection limit of 12 nM. Importantly, the practical application of **RhoSe** for Hg^{2+} detection was successfully demonstrated through test strips, live cell images, and live zebrafish images. **RhoSe** has been developed as a useful tool for monitoring Hg^{2+} distribution in biological samples.

Acknowledgements

Notes and references

1 G. Chen, Z. Guo, G. Zeng and L. Tang, *Analyst*, 2015, **140**, 5400–5443.
2 X. Li, X. Gao, W. Shi and H. Ma, *Chem. Rev.*, 2014, **114**, 590–659.

3 J. Wu, B. Kwon, W. Liu, E. V. Anslyn, P. Wang and J. S. Kim, *Chem. Rev.*, 2015, **115**, 7893–7943.

4 X. Chen, T. Pradhan, F. Wang, J. S. Kim and J. Yoon, *Chem. Rev.*, 2012, **112**, 1910–1956.

5 W. F. Fitzgerald, C. H. Lamborg and C. R. Hammerschmidt, *Chem. Rev.*, 2007, **107**, 641–662.

6 Z. Zhang, D. Wu, X. Guo, X. Qian, Z. Lu, Q. Xu, Y. Yang, L. Duan, Y. He and Z. Feng, *Chem. Res. Toxicol.*, 2005, **18**, 1814–1820.

7 M. Harada, *Crit. Rev. Toxicol.*, 1995, **25**, 1–24.

8 Mercury update: impact on fish advisories, EPA fact sheet (EPA-823-S2-01-011), EPA, Office of Water, Washington, DC 2001, pp. 1–10.

9 X. Chai, X. Chang, Z. Hu, Q. He, Z. Tu and Z. Li, *Talanta*, 2010, **82**, 1791–1796.

10 Y. Gao, S. De Galan, A. De Brauwere, W. Baeyens and M. Leermakers, *Talanta*, 2010, **82**, 1919–1923.

11 J. Wang, J. Lu, S. B. Hocevar, P. A. Farias and B. Ogorevc, *Anal. Chem.*, 2000, **72**, 3218–3222.

12 F. Moreno, T. Garcia-Barrera and J. L. Gomez-Ariza, *Analyst*, 2010, **135**, 2700–2705.

13 S. Atilgan, T. Ozdemir and E. U. Akkaya, *Org. Lett.*, 2010, **12**, 4792–4795.

14 J. Du, J. Fan, X. Peng, P. Sun, J. Wang, H. Li and S. Sun, *Org. Lett.*, 2010, **12**, 476–479.

15 Z. Guo, W. Zhu, M. Zhu, X. Wu and H. Tian, *Chem.–Eur. J.*, 2010, **16**, 14424–14432.

16 H. Yu, Y. Xiao, H. Guo and X. Qian, *Chem.–Eur. J.*, 2011, **17**, 3179–3191.

17 B. N. Ahamed and P. Ghosh, *Dalton Trans.*, 2011, **40**, 12540–12547.

18 C.-Y. Li, F. Xu, Y.-F. Li, K. Zhou and Y. Zhou, *Anal. Chim. Acta*, 2012, **717**, 122–126.

19 X. Ma, J. Wang, Q. Shan, Z. Tan, G. Wei, D. Wei and Y. Du, *Org. Lett.*, 2012, **14**, 820–823.

20 M. Vedamalai and S.-P. Wu, *Org. Biomol. Chem.*, 2012, **10**, 5410–5416.

21 J. Hu, Z. Hu, S. Liu, Q. Zhang, H. Gao and K. Uvdal, *Sens. Actuators, B*, 2016, **230**, 639–644.

22 Z. Yu, Z. Tian, Z. Li, Z. Luo, Y. Li, Y. Li and J. Ren, *Sens. Actuators, B*, 2016, **223**, 172–177.

23 M. Hong, X. Lu, Y. Chen and D. Xu, *Sens. Actuators, B*, 2016, **232**, 28–36.

24 P. Piyanuch, S. Watpathomsub, V. S. Lee, H. A. Nienaber and N. Wanichacheva, *Sens. Actuators, B*, 2016, **224**, 201–208.

25 B. Jurado-Sanchez, A. Escarpa and J. Wang, *Chem. Commun.*, 2015, **51**, 14088–14091.

26 H. N. Kim, M. H. Lee, H. J. Kim, J. S. Kim and J. Yoon, *Chem. Soc. Rev.*, 2008, **37**, 1465–1472.

27 M. Li, Y. Sun, L. Dong, Q.-C. Feng, H. Xu, S.-Q. Zang and T. C. W. Mak, *Sens. Actuators, B*, 2016, **226**, 332–341.

28 D. Zhang, M. Li, Y. Jiang, C. Wang, Z. Wang, Y. Ye and Y. Zhao, *Dyes Pigm.*, 2013, **99**, 607–612.

29 M. Wang, J. Wen, Z. Qin and H. Wang, *Dyes Pigm.*, 2015, **120**, 208–212.

30 K. C. Behera and B. Bag, *Dyes Pigm.*, 2016, **135**, 143–153.

31 S. Erdemir, M. Yuksekogul, S. Karakurt and O. Kocyigit, *Sens. Actuators, B*, 2017, **241**, 230–238.

32 H. Ding, C. Zheng, B. Li, G. Liu, S. Pu, D. Jia and Y. Zhou, *RSC Adv.*, 2016, **6**, 80723–80728.

33 C. Kumari, D. Sain, A. Kumar, S. Debnath, P. Saha and S. Dey, *RSC Adv.*, 2016, **6**, 62990–62998.

34 J. Luo, S. Jiang, S. Qin, H. Wu, Y. Wang, J. Jiang and X. Liu, *Sens. Actuators, B*, 2011, **160**, 1191–1197.

35 Y. Wang, H. Wu, J. Luo and X. Liu, *React. Funct. Polym*, 2012, **72**, 169–175.

36 D. S. McClure, *J. Chem. Phys.*, 1951, **20**, 682–686.

37 R. K. Zalups, *Pharmacol. Rev.*, 2000, **52**, 113–144.

38 B. F. Azevedo, L. B. Furieri, F. M. Pecanha, G. A. Wiggers, P. F. Vassallo, M. R. Simoes, J. Fiorim, P. R. de Batista, M. Fioresi, L. Rossoni, I. Stefanon, M. J. Alonso, M. Salaices and D. V. Vassallo, *J. Biomed. Biotechnol.*, 2012, 1–11.

39 V. Dujols, F. Ford and A. W. Czarnik, *J. Am. Chem. Soc.*, 1997, **119**, 7386–7387.

40 S.-R. Liu and S.-P. Wu, *Org. Lett.*, 2013, **15**, 878–881.

41 H. A. Benesi and J. H. Hildebrand, *J. Am. Chem. Soc.*, 1949, **71**, 2703–2707.